JOURNAL OF SPACECRAFT AND ROCKETS
Vol. 44, No. 2, March–April 2007

Analysis of Increased Compression Through Area Constriction on Ejector-Rocket Performance

J. Etele*
Carleton University, Ottawa, Ontario K1S 5B6, Canada
B. Parent†
Nagaoka University of Technology, Nagaoka 940-2188, Japan
and
J. P. Sislian‡
University of Toronto, Toronto, Ontario M3H 5T6, Canada

DOI: 10.2514/1.26915

The use of an ejector as part of a larger rocket-based propulsive device is investigated in terms of increasing thrust as compared to a pure rocket system. A theoretical framework is presented to establish the relation between increasing ejector compression and increasing thrust, whereas numerical simulations are presented to demonstrate the viability of using area constriction to achieve increased ejector compression. Using a constant length ejector, the exit area is constricted by between 12 and 25% and compared to a similarly configured unconstricted ejector. In addition, both a purely conical and a conical/cylindrical constriction configuration are examined, in which an increase of 30% in the ejector compression ratio is achieved in the best case.

Nomenclature

A	=	area
a	=	speed of sound
C_p	=	specific heat at constant pressure
I_{sp}	=	specific impulse
k	=	specific turbulence kinetic energy
$\mathcal{M}$	=	molecular weight
$\dot{m}$	=	mass flow rate
p	=	pressure
R	=	gas constant
$\bar{R}$	=	universal gas constant, 8.314 kJ/kmol · K
r	=	radial coordinate
T	=	temperature
$\mathcal{T}$	=	thrust
t	=	time
u	=	streamwise velocity component
x	=	streamwise coordinate
α	=	air/rocket mass flow ratio
γ	=	ratio of specific heats
δ	=	boundary layer height
ζ	=	rocket/air total pressure ratio, p_r^o/p_a^o
θ	=	air/rocket specific total enthalpy ratio
π_m	=	compression ratio, p_m^o/p_a^o
$\bar{\pi}_m$	=	compression augmentation
σ	=	rocket exhaust/ejector inlet area ratio
Φ	=	thrust augmentation ratio
ϕ	=	equivalence ratio
ω	=	dissipation rate per unit of k

Subscripts

A	=	annular
a	=	air
ave	=	average
axi	=	inviscid axisymmetric terms
C	=	central
e	=	exit
m	=	mixed
p	=	pressure
r	=	rocket
T	=	turbulent
v	=	viscous
Δm	=	change in momentum
∞	=	freestream

Superscripts

o	=	stagnation conditions
$*$	=	sonic conditions

Introduction

ONE way of incorporating the benefits of air breathing into rocket-based launch vehicles is through the use of an ejector system. This idea is central to the development of rocket-based combined cycle (RBCC) engines, in which it is the ejector effect that is primarily responsible for any increased performance over traditional rocket systems during the initial phases of launch. A typical RBCC engine would transition between 1) ejector, 2) ramjet, 3) scramjet, and 4) pure rocket modes. However, even in the absence of high-speed propulsive modes that include the combustion of atmospheric oxygen (i.e., ramjet and/or scramjet operation), an RBCC with an ejector mode has the potential to improve performance through the entrainment and compression of atmospheric air, especially at low speeds. Therefore, the focus of this work is to illustrate a potential means of increasing the performance of the ejector mode itself, where it is implied that improving this single component within the larger RBCC engine system could lead to improved overall performance.

The thrust augmenting potential of ejectors has been studied as far back as 1949 with the work of Von Kármán [1]. This type of theoretical treatment is often focused on accurately estimating the air inflow conditions under the various ejector operating regimes (see

Received 2 August 2006; accepted for publication 1 November 2006. Copyright © 2006 by Jason Etele. Published by the American Institute of Aeronautics and Astronautics, Inc., with permission. Copies of this paper may be made for personal or internal use, on condition that the copier pay the $10.00 per-copy fee to the Copyright Clearance Center, Inc., 222 Rosewood Drive, Danvers, MA 01923; include the code 0022-4650/07 $10.00 in correspondence with the CCC.

*Assistant Professor, Department of Mechanical and Aerospace Engineering, 1125 Colonel By Drive; jetele@mae.carleton.ca. Member AIAA.

†JSPS Researcher, 1603-1 Kamitomioka; bernard.parent@utoronto.ca.

‡Professor, Institute of Aerospace Studies, High Speed Vehicle Propulsion Group, 4925 Dufferin Street; sislian@caius.utias.utoronto.ca. Associate Fellow AIAA.

Fabri and Siestrunck [2]), because the ratio of entrained air to rocket exhaust mass flows, also referred to as the entrainment ratio α, is a key operating parameter. Dutton and Carroll [3,4] examine ejector configurations in which, in addition to the entrainment ratio, other relevant parameters such as the compression ratio (the ratio of the total pressure at the ejector exit plane to that of the entrained air, π_m) are maximized.

These two ejector parameters, α and π_m, define a given ejector's performance. Because $\alpha = 0$ represents a pure rocket, a minimum value for this parameter is required for an ejector-rocket engine to be considered "air-breathing." Given the ejector's main function as a jet pump, the maximization of the compression ratio is also a key performance indicator, even in applications where the ejector is used in nonpropulsive systems (Emanuel [5]).

To improve the accuracy of theoretical treatments for lower entrainment ratios while also providing a means of determining the flow details within the ejector section itself (not simply at the inflow and outflow planes), Chow and Addy [6] developed a method in which one can approximate the viscous effects within the shear layer between the air and rocket streams. This allows for an estimation of the mass flow passing through the mixing layer to be added to the entrained air mass flow calculated based on the assumption of no mixing up to the point at which the airflow chokes. They also show that the theory provides a reasonable estimation of the wall pressure within the ejector as compared to experimental results, whereas Chow and Yeh [7] show that this theory can be extended to ejectors where the outer wall profile is parabolic in the streamwise direction (in addition to a constant area ejector). At higher entrained air mass flow rates, Peters et al. [8] developed a method that accounts for the effects of turbulence within the mixing layer as well as allowing for equilibrium chemical reactions to occur within the ejector section (as would be expected when the core rocket is operating under fuel-rich conditions). The inclusion of chemical reactions and hence heat release during the mixing process forces the ejector into an operating regime where the entrainment ratio is no longer dominated by the choking of the unmixed entrained air. This mode of operation is also examined by Masuya et al. [9] where chemical equilibrium calculations are added to a 1-D flow model using an experimentally determined wall pressure distribution.

In addition to theoretical treatments, there have been numerous numerical studies outlining the potential benefits and performance of various combined cycle technologies (Escher [10], Escher and Schnurstein [11], Nix and Escher [12], Daines and Segal [13], Billig [14], Fink [15], Ramette et al. [16], Dorrington [17]). Of particular interest to this work are those studies in which the flowfield within ejectors has been examined numerically, especially as it relates to the incorporation of the ejector within the larger class of RBCC engines. Matesanz et al. [18], using an explicit, finite element based algorithm and a $k\varepsilon$ turbulence model, examine a simple axisymmetric ejector with a single rocket placed along the axis. West et al. [19] and Ruf [20] examine a similar configuration but with the addition of downstream hydrogen injection (as would occur in an RBCC engine operating in a diffusion and afterburning mode; see Daines and Segal [13]) using a pressure-based reacting flow solver (seven species, nine reaction, H_2/O_2) and an extended $k\varepsilon$ turbulence model. A similar ejector configuration and numerical solution routine are used by Jahingir and Huque [21], where the numerical results form part of a broader optimization study to determine the optimal combination of ejector design variables that simultaneously maximize α, π_m, and the ejector nozzle efficiency.

In efforts to improve on this design, rocket placement within an ejector duct has also been studied. At the Pennsylvania State University, Cramer et al. [22] used hot rocket exhaust combined with diffusion and afterburning in the downstream sections of an RBCC engine to compare the effect of using twin thrusters to a single thruster within a rectangular geometry. This experimental study found that the twin thruster configuration could entrain more air, mix in a shorter distance, and produce higher compression ratios than the single thruster configuration. The present authors also studied the effect of rocket placement within an axisymmetric, constant area ejector [23] using an implicit, finite difference code solving the Favre-averaged Navier–Stokes equations with the Wilcox $k\omega$ turbulence model (including the Wilcox dilatational dissipation correction). It was found that a configuration that used both an annular rocket along the outer wall of the ejector in addition to a rocket located along the axisymmetric axis (Fig. 5, in which the rocket exhaust mass flow is biased 3:1 in favor of the annular rocket) is able to achieve compression ratios as high as 2.5 for the case in which both the entrained air and rocket exhaust mass flows are equal.

Rocket configuration is also identified as a means of improving ejector performance by Makaron and Fedyayev [24], where not only the placement of the nozzles, but the angle of their exhaust relative to the entrained air is examined. This idea is similar to that used at the Brigham Young University by Daines [25] and Daines and Bulman [26], where a CFD study of a straight, rectangular ejector duct was done using a pressure-based predictor–corrector algorithm incorporating the $k\epsilon$ two-equation turbulence model of Chen and Kim. However, in addition to simply fixing the rocket exhaust angle for a given simulation, a Crank–Nicholson scheme was used to obtain time-accurate solutions involving the dynamic switching of the rocket exhaust angle. This study found that the time-averaged value of thrust was increased by 32% for a sine wave switching mode (3000 Hz), whereas the use of a square wave switching mode produced increases as high as 52% (1500 Hz) when compared to a similarly configured steady flow ejector. The major influence on the increased thrust was found to be the creation of accelerated air pockets, where the rate at which these pockets were expelled from the ejector was found to have a significant impact on the overall thrust. In addition to increased levels of thrust, it was also reported that the dynamic operation of the ejector increased the entrained air mass flow rate by nearly 75% compared to a steady flow ejector. However, it was also reported that the alternating pockets of high-speed flow created segregated mixture regions (as indicated by the species mass fractions), indicating poor mixing of the two streams.

To this point, most of the research aimed at improving ejector performance has dealt with constant area ejector configurations. However, there exists experimental evidence (Makaron and Fedyayev [24]) which indicates that the ejector duct itself can be modified to potentially improve performance as per the suggestion of others (Escher and Schnurstein [11]). Therefore, it is the objective of this paper to demonstrate that exit area constriction can be used to effectively increase the compression ratio of a constant length axisymmetric ejector. A theoretical framework is used to demonstrate that increased compression is more beneficial than increased air mass flow, whereas numerical simulations are used to demonstrate the feasability of using exit area constriction as a means of obtaining this desired increase in compression.

Ejector Theory

There are two phases of operation during acceleration for an ejector engine using the jet compression process, differentiated by the behavior of the incoming air. During the initial stages of launch when the flight Mach number is subsonic, the incoming air is entrained into the ejector duct by the action of the rocket exhaust. This pumping action acts to increase the total mass flow through the ejector duct and the engine can be said to be operating in *ejector-rocket* or simply *ejector* mode. However, as the flight Mach number is increased to values beyond Mach 1, the air inflow is generally determined by external conditions such as flight Mach number and inlet shock structure (unless at some downstream point within the ejector the conditions are sufficient to unstart the inlet). In this case, the engine is sometimes considered to be operating in *air augmented rocket* or *ram rocket* mode. However, in each of these two conditions the engine is relying on the jet compression process and it is simply the manner in which the entrained air mass flow is determined that varies.

At subsonic speeds, the critical performance parameter is the incoming air Mach number M_a, as it is this air-breathing aspect of the ejector that offers improved performance over pure rocket systems. To determine this value, it is often convenient to assume an aerodynamic choking condition, where due to the expansion of the

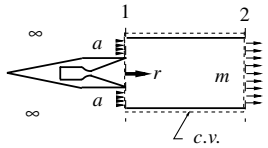

Fig. 1 Ejector section of an ejector/rocket or RBCC engine.

high pressure rocket exhaust into the entrained airstream, the subsonic incoming air encounters a converging area streamtube and hence accelerates towards Mach 1 (Aoki et al. [27], Kanda and Kudo [28], Etele et al. [23]). However, this presupposes two conditions: 1) the static pressure in the rocket exhaust is sufficiently higher than that in the entrained air stream at the ejector inlet so as to create a converging air streamtube, and 2) the conditions downstream of the ejector are such that they do not influence the conditions at the inlet. This can lead to a restriction in the variety of scenarios that can be examined, especially those where conditions further downstream can have a significant impact on the entrained airflow (i.e., processes such as heat addition through combustion or area constriction). Under these circumstances, a more general model is required and used herein. For a control volume surrounding the ejector section (Fig. 1) the conservation of momentum principle yields

$$\dot{m}_r u_r + p_r A_r + \dot{m}_a u_a + p_a A_a = \dot{m}_m u_m + p_m A_m \tag{1}$$

Following the method outlined in [23], if one defines

$$\chi(\gamma, M) = \frac{M + 1/(\gamma M)}{\sqrt{2/(\gamma+1) + [(\gamma-1)/(\gamma+1)]M^2}} \tag{2}$$

then Eq. (1) can be rewritten as

$$\dot{m}_r a_r^* \chi_{(a,1)} + \dot{m}_a a_a^* \chi_{(a,1)} = \dot{m}_m u_m + p_m A_m \tag{3}$$

where the subscripts on χ denote the stream under consideration (to determine the value of γ to be used) followed by the location of interest (for determining Mach number). In writing Eq. (3) one has also made use of the sound speed at $M = 1$ which is related to the total temperature of the fluid through

$$a^{*2} = 2\frac{\gamma-1}{\gamma+1} C_p T^o \tag{4}$$

Considering the right side of Eq. (3), noting that $\dot{m} = \rho u A$ while applying the perfect gas law to express density as a function of temperature and pressure, one can use the definition of Mach number and rearrange to obtain

$$M_m^2 = \frac{1}{\gamma_m}\left\{\frac{\dot{m}_r a_r^*}{p_m A_m}(\chi_{(r,1)} + \alpha\Gamma_{(a,r)}\sqrt{\theta}\chi_{(a,1)}) - 1\right\}$$

where

$$\alpha = \frac{\dot{m}_a}{\dot{m}_r}, \qquad \theta = \frac{C_{pa} T_a^o}{C_{pr} T_r^o} \tag{5}$$

and

$$\Gamma_{(a,r)} = \sqrt{\frac{(\gamma_a - 1)(\gamma_r + 1)}{(\gamma_a + 1)(\gamma_r - 1)}} \tag{6}$$

This can be further simplified by using the definition of a_r^* [Eq. (4)] and writing the mass flow as

$$\frac{\dot{m}}{A} = \left(\frac{p^o}{\sqrt{RT^o}}\right)\mu \tag{7}$$

where μ is defined as

$$\mu(\gamma, M) = \sqrt{\gamma} M \left(1 + \frac{\gamma-1}{2}M^2\right)^{[-(\gamma+1)]/[2(\gamma-1)]} \tag{8}$$

to obtain (assuming a constant area ejector)

$$M_m^2 = \frac{1}{\gamma_m}\left\{\mu_{(r,1)}\sigma\left(\frac{p_r^o}{p_m}\right)\sqrt{\frac{2\gamma_r}{\gamma_r+1}}[\chi_{(r,1)} + \alpha\Gamma_{(a,r)}\sqrt{\theta}\chi_{(a,1)}] - 1\right\} \tag{9}$$

where

$$\sigma = \frac{A_r}{A_r + A_a} \tag{10}$$

Applying the principle of mass conservation through the ejector, one can write

$$\dot{m}_r(\alpha + 1) = p_m A_m \sqrt{\frac{\gamma_m}{R_m T_m^o}} M_m \left(1 + \frac{\gamma_m - 1}{2} M_m^2\right)^{\frac{1}{2}} \tag{11}$$

where in addition to the Mach number of the mixed flow, the ratio of specific heats at this location is also introduced. This, and other fluid properties at the ejector mixed flow plane, can be determined on a mixing rule basis (assuming complete mixing) using

$$\mathcal{M}_m = \frac{1}{\alpha+1}(\alpha\mathcal{M}_a + \mathcal{M}_r) \qquad \gamma_m = \frac{1}{\alpha+1}(\alpha\gamma_a + \gamma_r)$$
$$C_{pm} = \frac{\gamma_m}{\gamma_m - 1}\left(\frac{\bar{R}}{\mathcal{M}_m}\right) \tag{12}$$

For a steady, inviscid, adiabatic mixing process within the ejector, the conservation of energy equation can be rearranged using the definitions in Eq. (5) to yield the relation

$$\frac{C_{pm} T_m^o}{C_{pr} T_r^o} = \frac{\alpha\theta + 1}{\alpha + 1} \tag{13}$$

which in turn can be used to simplify Eq. (11) to yield

$$\mu_{(m,2)}\left(1 + \frac{\gamma_m - 1}{2} M_m^2\right)^{(\gamma_m+1)/(\gamma_m-1)}$$
$$= \mu_{(r,1)}\sigma\left(\frac{p_r^o}{p_m}\right)\Upsilon_{(r,m)}\sqrt{(\alpha\theta+1)(\alpha+1)} \tag{14}$$

where

$$\Upsilon_{(r,m)} = \sqrt{\frac{\gamma_r(\gamma_m - 1)}{\gamma_m(\gamma_r - 1)}} \tag{15}$$

When the stagnation conditions, the ejector inlet geometry, and the rocket exhaust Mach number entering the ejector are all known quantities (T_a^o, T_r^o, p_a^o, p_r^o, σ, and M_r), in addition to the gas composition of both the rocket and airstreams (γ_a, γ_r, C_{pa}, and C_{pr}), then there remain only three unknowns in Eqs. (9) and (14). Two of these unknowns are Mach numbers, the first being the Mach number of the entrained airstream M_a (needed to solve both $\chi_{(a,1)}$ and $\mu_{(a,1)}$), whereas the second is that of the mixed flow M_m. The third unknown is the mixed flow pressure p_m, which reflects the fact that information downstream in the engine can influence the properties at the ejector inlet (unlike the case of a choked entrained airstream where the necessity of prescribing a downstream parameter is eliminated through the assumption of $M_a = 1$ shortly after entering the ejector).

Therefore, for a given mixed flow pressure, Eqs. (9) and (14) represent a system of two equations and two unknowns that can be readily solved. Because M_m appears as a squared term in both equations, the result will be two possible solutions for a given mass flow ratio α. However, the additional constraint of a specific mixed flow pressure will uniquely determine which of the two Mach number solutions is obtained (high static pressure = subsonic mixed flow, low static pressure = super sonic mixed flow).

For an engine in which an ejector is employed (illustrated schematically in Fig. 2), to calculate the thrust obtainable for a particular set of conditions one can write

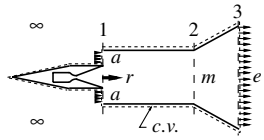

Fig. 2 Control Volume (c.v.) surrounding entire propulsive system.

$$\mathcal{T} = \underbrace{A_e(p_e - p_\infty) - A_a(p_a - p_\infty)}_{\mathcal{T}_p} + \underbrace{\dot{m}_r[(\alpha+1)u_e - \alpha u_a]}_{\mathcal{T}_{\Delta m}} \quad (16)$$

where both the pressure forces and the change in momentum contribute to the propulsive force of the engine. For a control volume surrounding the entire engine as shown in Fig. 2, if one assumes isentropic flow from ∞ to 1 and from 2 to 3 (i.e., everywhere but within the ejector itself) then $p_\infty = p_a^o$ and $p_m^o = p_e^o$, allowing one to write, for the pressure component of thrust,

$$\mathcal{T}_p = A_m p_a^o \left\{ \frac{\mu_{(m,2)}}{\mu_{(m,3)}} \left(\frac{p_e}{p_a^o} - 1 \right) + (\sigma - 1) \left[\left(1 + \frac{\gamma_a - 1}{2} M_a^2 \right)^{-\gamma_a/(\gamma_a - 1)} - 1 \right] \right\} \quad (17)$$

where it is also assumed that the mixing process is completed by the end of the ejector (station 2) thus $\gamma_m = \gamma_e$. Specifying the mixed flow static pressure yields M_a as previously described, while setting the exit plane pressure p_e yields the flow Mach number leaving the engine through:

$$M_e^2 = \frac{2}{\gamma_m - 1} \left[\left(\frac{\pi_m p_a^o}{p_e} \right)^{(\gamma_m - 1)/\gamma_m} - 1 \right] \quad (18)$$

where here the compression ratio has been introduced, which represents the ratio of mixed flow to entrained air total pressures:

$$\pi_m = \frac{p_m^o}{p_a^o} \quad (19)$$

It should be noted that in specifying both p_m and p_e, it is implied that the nozzle shape is variable. Because the nozzle entrance area (which is the same as the ejector exit area) is a set parameter, under the assumption of isentropic flow through the nozzle [Eq. (18)], there is a unique area ratio required to produce the given exit pressure. Therefore, for a given p_m, as the exit pressure is varied, the area ratio between stations 2 and 3 in Fig. 2 changes. In fact, for cases where p_m is high and $M_m < 1$, a low exit pressure requires the flow through the nozzle to go from subsonic to supersonic speeds, thereby implying a converging/diverging nozzle shape from station 2 to 3.

Under the same assumptions as used for $\mathcal{T}_p$, the component of thrust due to the change in momentum through the engine can be expressed as

$$\mathcal{T}_{\Delta m} = A_r p_r^o \mu_{(r,1)} \times \left\{ \begin{array}{c} \sqrt{(\alpha\theta + 1)(\alpha + 1)}\,\Upsilon_{(r,e)} M_e \sqrt{\gamma_m} \left(\frac{\mu_{(m,3)}}{M_e \sqrt{\gamma_m}} \right)^{(\gamma_m - 1)/(\gamma_m + 1)} \\ + \alpha \sqrt{\theta}\,\Upsilon_{(r,a)} M_a \sqrt{\gamma_a} \left(\frac{\mu_{(a,1)}}{M_a \sqrt{\gamma_a}} \right)^{(\gamma_a - 1)/(\gamma_a + 1)} \end{array} \right\} \quad (20)$$

With Eqs. (17) and (20) one can now calculate the total thrust of a rocket-ejector engine specifying only two variables, the static pressure at the end of the ejector section and at the engine exit plane (p_m and p_e, respectively). Additionally, the thrust of a pure rocket can be found by setting $A_a = \alpha = 0$ (i.e., a pure rocket will have no air entrainment area and hence no mass flow of air), where it is assumed that the frontal area of the rocket equals the nozzle exit area. The increase in thrust using a rocket ejector as compared to a rocket alone can then be evaluated using the thrust augmentation ratio:

$$\Phi = \frac{\mathcal{T}_{\text{ejector}}}{\mathcal{T}_{\text{rocket}}} \quad (21)$$

Theoretical Analysis

In addition to simply entraining atmospheric air, an ejector must also act on this air in a manner that increases the potential thrust obtainable from the flow leaving the ejector section. In cases where the ejector rocket is used on its own without any further fuel addition (i.e., in an application similar to that shown in Fig. 2), increasing the compression ratio can have a significant impact on engine performance.

To assess this impact, a kerosene-fueled rocket configuration will be used to represent a rocket typical of the first stage of a launch engine. Table 1 lists two sets of rocket parameters, one representative of an Atlas E/F first stage (based on the Rocketdyne MA-3 engine) which is used in all the theoretical calculations, and another that is used in the numerical computations. The values listed are obtained using an equilibrium combustion calculation and a nozzle design method (see [29]), where the values of equivalence ratio and the stagnation conditions for the Atlas E/F engine are determined by matching an estimated value of I_{sp}.

In addition to specifying the rocket parameters, the flight conditions are also required to determine ejector performance. Two operating conditions are chosen, where the beginning of a launch cycle is represented by a static sea level condition and a condition just before the point at which the vehicle reaches Mach 1 is chosen as a representative location where past which (i.e., higher and faster) the theoretical method for calculating the entrained air mass flow would begin to lose its validity (as the air inflow conditions would begin to be dominated by the supersonic inflow). These two conditions are listed in Table 2 along with the resulting ejector parameters as calculated with a given rocket configuration. It should be noted that the increase in ζ is due primarily to the decrease in the freestream total pressure as the altitude is increased, not the change in rocket total pressure (where it is the generic rocket configuration that is evaluated at the higher altitude condition).

With the variables listed in Tables 1 and 2 for the Atlas E/F engine, all the required information to apply the previously described theory is known except for the mixed flow pressure and the exit pressure (it should be noted that the Atlas E/F exit conditions are set so as to obtain a static pressure ratio between the rocket exhaust and entrained air streams of unity at the ejector inlet). The mixed flow pressure is used to control the entrained air mass flow rate and thus closes the solution for a particular ejector condition. The remaining

Table 1 Rocket configurations

Variable	Atlas E/F[a]	Generic engine
Fuel	Kerosene	Kerosene
ϕ	1.49	0.20
p_r^o, MPa	4.86 (48 atm)	5.87 (58 atm)
T_r^o, K	3668	2316
γ	1.22	1.27
I_{sp}, s (vacuum)	240 (336)	187 (203)

[a]Approximations based on theoretical calculations.

Table 2 Ejector operating parameters

Variable	Atlas E/F	Generic Engine
Altitude, m	Sea level	8000
M_∞	0	0.8
p_a^o, kPa	101.3	58.7[a]
T_a^o, K	288	279
σ	0.10	0.10
θ	0.038	0.09
$\zeta = p_r^o / p_a^o$	48	100

[a]For numerical simulations, $p_a^o / p_\infty^o = 0.85$.

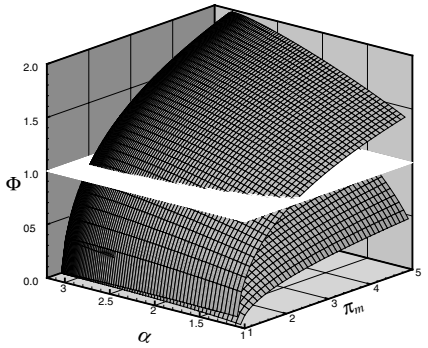

Fig. 3 Thrust augmentation for an ejector based on an Atlas E/F launch rocket (static sea level conditions, $p_e = 100$ kPa). Upper surface = subsonic, lower surface = supersonic.

unknown, the rocket-ejector exit pressure, is set to 100 kPa to evaluate the total thrust produced by the engine.

Figure 3 shows the theoretical thrust augmentation results with both a subsonic and supersonic mixed flow at the ejector exit plane. Although these surfaces represent the complete range of possible solutions, only those configurations that yield $\Phi > 1$ actually increase the thrust produced over the same rocket used in isolation. A subsonic mixed flow produces the largest region of solutions above the $\Phi = 1$ plane, where not only is this region reduced in size for the supersonic solution, but the minimum value of π_m required to simply match the stand-alone rocket thrust is increased over that required for a subsonic mixed flow at the same value of α. In both cases it can be seen that increasing the entrainment ratio increases the thrust augmentation; however, there exists a limit at the point where both the subsonic and supersonic solutions converge (at which point the entrainment ratio reaches a maximum of approximately 3.2).

In terms of the compression ratio, for both the subsonic and supersonic conditions, increasing π_m within the ejector section increases the overall thrust augmentation. One possible means of obtaining this increase is through the use of area constriction. However, the use of a reduced mixed flow area implies a reduced value of α compared to a similarly configured straight ejector, because the rocket conditions are fixed, leaving only the entrained air mass flow to decrease. In turn, the consequential decrease in α will yield a *decrease* in the thrust augmentation, thereby creating the need to asses which of these two variables, α or π_m, would be more beneficial to increase. For this purpose the results in Fig. 3 are reduced to a 2-D α–π_m plane in Fig. 4.

Using the previously described ejector theory, the solid line represents the set of solutions for the case of a straight ejector, where at a given α a fully mixed flow yields the particular compression ratio indicated (the left branch represents a subsonic mixed flow solution, the right a supersonic mixed flow). The two broken lines represent the intersection of a given Φ plane with the solution surface in Fig. 3, in which both the $\Phi = 1.0$ and $\Phi = 1.1$ traces are shown. If one starts with a straight ejector at an entrainment ratio of 1.5 as indicated by the solid circle in Fig. 4, one can see that the resulting thrust is less

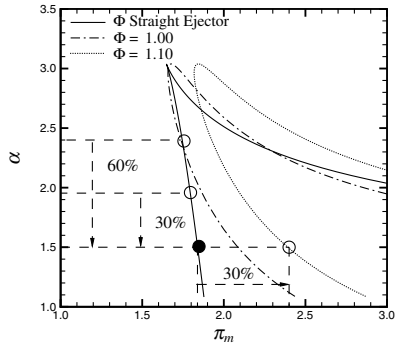

Fig. 4 Effect of changing α and π_m on thrust augmentation (Atlas E/F, static sea level conditions, $p_e = 100$ kPa).

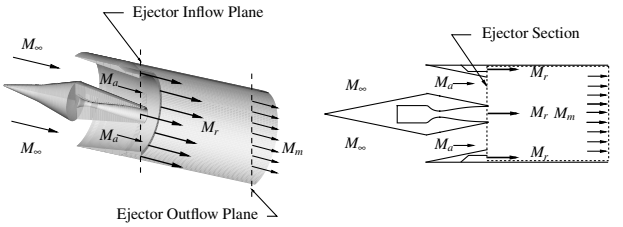

a) $75_A/25_C$ Rocket exhaust **b) Computational domain**

Fig. 5 Base (unconstricted) ejector configuration.

than that of the stand-alone rocket (i.e., it lies to the left of the $\Phi = 1.0$ curve). However, if one constricts the ejector area so as to achieve a 30% increase in the compression ratio, it is possible to produce a 10% increase in thrust as shown by the open circle on the $\Phi = 1.1$ curve. If the constricted ejector is operating at maximum mass flow conditions (i.e., the flow is choked), this implies that the equivalent straight ejector is operating at less than maximum entrained air capacity and could in fact yield a mass flow ratio in excess of 1.5. If the constriction required to achieve this 30% increase in the compression ratio results in a 30% reduction in α, restoring this mass flow of air to the straight ejector still yields a net decrease in thrust as compared to the rocket alone (i.e., the point still lies to the left of the $\Phi = 1.0$ curve). In fact, as shown in Fig. 4, even if the ejector constriction required to obtain a 30% increase in π_m produces a 60% decrease in the mass flow ratio, one would still obtain a net result better than the straight ejector. Under these conditions the straight ejector would just barely produce thrust equivalent to the rocket alone, whereas the constricted ejector with 60% less entrained air would yield a 10% increase in thrust.

Therefore, to evaluate the increase in compression and the resulting decrease in entrained air mass flow obtainable through area constriction, the straight ejector configuration as shown in Fig. 5 will be modified and solved numerically (which represents the portion of the engine between stations 1 and 2 in Fig. 2).

Computational Results

The flowfield within an ejector as illustrated in Fig. 5 is solved using the axisymmetric, multispecies, Favre-averaged Navier–Stokes (FANS) equations combined with the Wilcox $k\omega$ turbulence model (including the Wilcox dilatational dissipation correction) in generalized curvilinear form using Window Allocatable Resolver for Propulsion (WARP) [30,31]. This codes uses an implicit Euler time-marching scheme incorporating block implicit factorization to iterate towards a steady-state solution using a pseudo-time-step determined from a combination of both the minimum and maximum Courant–Friedrichs–Lewy (CFL)-based local time step conditions. The convective terms are treated using the Roe scheme in conjunction with Yee flux limiters while the diffusive terms are treated with a second-order accurate, centered, finite differencing stencil. Convergence is judged against the magnitude of both the continuity and energy residuals. Details of the form of the flux vectors and the validation of this code on other nonaxisymmetric high-speed flows can be found in [23,32], whereas its application to axisymmetric flows has been tested in [29]. In flux vector form the governing equations can be expressed as

$$\frac{\partial Q}{\partial t} + \frac{\partial E}{\partial x} + \frac{\partial F}{\partial r} + S_{\text{axi}} - S_{k\omega} - \frac{\partial E_v}{\partial x} - \frac{\partial F_v}{\partial r} - S_{\text{axi}_v} = 0 \qquad (22)$$

For all the configurations presented, the results are obtained on a 2-D grid approximately 600×150, with clustering around the rocket walls protruding into the ejector section. For the conical/cylindrical configurations, clustering at the location where the configuration changes from conical to cylindrical is added such that the streamwise grid spacing is approximately 1 mm (see Fig. 6). Reference [23] contains the details of a grid convergence study done for the base configuration, where it was found that although differences of approximately 10% were found between the mass-flow-averaged

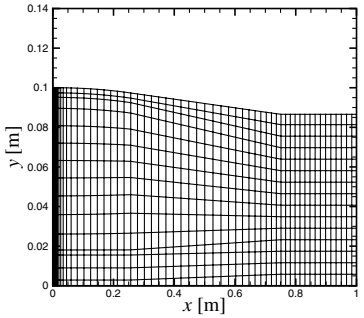

Fig. 6 Computational grid for the conical/cylindrical configuration with a 25 cm cylindrical section (every tenth grid line shown).

compression ratio in going from a grid of dimensions 517×150 to 2000×450 (an 11-fold increase in grid density), this error was on the conservative side in that the smaller grids underpredict π_m.

The total length of all the ejectors considered is 1.0 m, whereas the outer diameter at the ejector inflow plane is 0.2 m. Both the total pressure and total temperature are held constant at the air inflow boundary thus allowing the inflow Mach number to change, which in turn leaves the air mass flow rate free to adjust to the ejector flowfield. The rocket exhaust inflow boundary is uniform in the radial direction and supersonic, with the Mach number, static pressure, and static temperature specified (corresponding to a rocket exhaust Mach number of 3.1 with the total conditions as listed in Table 1 for the generic engine configuration). The outer wall of the ejector, as well as the 10 mm sections of rocket wall protruding into the ejector section, are specified as no-slip, adiabatic walls whereas the central axis boundary is symmetric. To avoid dividing by zero near the axisymmetric axis, an offset of 0.01 μm is applied along the length of the ejector. To control the overall ratio of air to rocket exhaust mass flows, the static pressure is set along the entire height of the ejector outflow plane in each case so as to produce a value for α as close as possible to 0.75. On a molar basis the air is modeled as 80% N_2, 20% O_2, whereas the rocket exhaust is composed of 76% O_2, 17% CO_2, and 7% H_2O. This corresponds to the equilibrium postcombustion mixture for kerosene and oxygen at an equivalence ratio of 0.2 based on the reaction

$$\phi C_{12}H_{24} + 18O_2 \rightarrow 12H_2O + 12CO_2 \tag{23}$$

Although the equivalence ratio is much lower than in typical rockets (as can be seen in comparison to the Atlas E/F), it is chosen such that no combustible species enter the ejector. This eliminates the possibility of simultaneous mixing and combustion and thus removes the requirement for a chemistry routine within the numerical solver. The turbulent Schmidt and Prandtl numbers are set to 1.0 and 0.5, respectively, whereas the freestream value of ω is set to 10 times the flow speed (both Pr_T and Sc_T along with the wall value of ω are set to the values recommended by Wilcox [33] for shear/mixing layers). The flowfields in all cases are judged converged when the residual has been reduced by approximately 8 orders of magnitude.

Base Configuration

To judge the effectiveness of area constriction, the base configuration as shown in Fig. 5 is used as a reference. This configuration was found to produce the highest levels of both mixing and compression when compared to an ejector with only a central rocket along the axis of symmetry and to configurations with smaller annular rockets [23]. With the annular rocket stream containing 75% of the total rocket exhaust entering the ejector, for the case where the ratio of air to rocket exhaust mass flows is 0.75, this configuration produces a compression ratio of approximately 2.25 over 95% of the total ejector area. It should be kept in mind that this is not the maximum compression ratio possible for this configuration, nor is the ejector operating under maximum mass flow conditions, but rather that these results pertain to an ejector where the back pressure is specified so as to obtain $\alpha = 0.75$.

This is best illustrated by the Mach number profiles in Fig. 7a, in which the effect of specifying the static pressure at the exit plane (to approximately 120 kPa) is to prevent the entrained airflow from reaching sonic velocity anywhere within the ejector section. This is in contrast to the case when no restraints are placed at the exit as shown in Fig. 7b, in which the expansion of the rocket exhaust into the airstream causes the airflow to choke at approximately the 50 cm location. Past this point, the mixing of the highly supersonic rocket exhaust and the sonic airflow produces a supersonic mixed flow at the exit, which in turn increases the compression ratio by approximately 10% and the mass flow ratio by approximately 30% to 2.5 and 1.0, respectively. Therefore, in relation to the assumptions made in the theoretical analyses with respect to the associated decrease in the entrained air mass flow that accompanies an area constriction, the constricted ejector configurations with $\alpha = 0.75$ experience an approximately 30% decrease in airflow as compared to the maximum possible value with the constriction removed.

With the base configuration established, it is possible to evaluate the effectiveness of a given constriction strategy in terms of its effect on the compression process. For clarity, each constricted case will be evaluated using the compression augmentation parameter, $\bar{\pi}_m$, which is simply the mass-flow-averaged compression ratio of the constricted configuration divided by that of the base case shown in Fig. 7a ($\pi_m = 2.25$). Therefore, for cases where constriction improves performance $\bar{\pi}_m > 1$ and $\pi_m > 2.25$.

Conical Configuration

To properly assess the effects of any area decrease on ejector performance, careful attention must be paid to ensuring uniformity of operating parameters between cases being compared. Although for all of the constricted cases considered in this paper both the

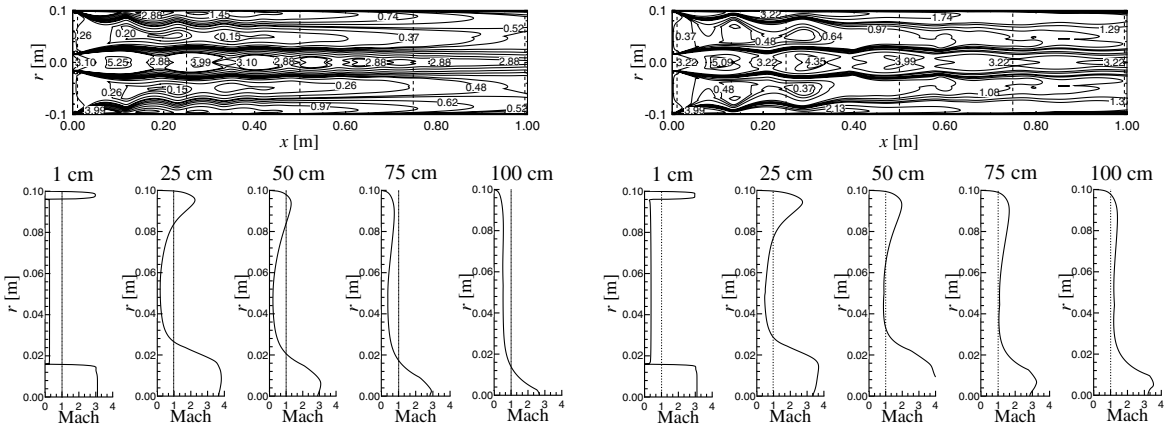

a) Set exit pressure (≈120 kPa) **b) No set exit pressure**

Fig. 7 Mach number contours for the base (unconstricted) configuration.

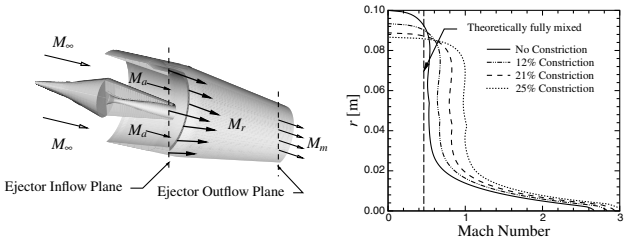

a) Conical constriction **b) Mach number profiles at exit plane**

Fig. 8 Conical flowfield configuration.

freestream and rocket conditions are held constant at the values in Tables 1 and 2, a decrease in exit area will decrease the allowable mass flow passing through the ejector, thereby decreasing α. However, as shown by the solid line in Fig. 4, independent of any effects due to area constriction, simply decreasing α will cause an increase in π_m. Thus if α is not kept constant between cases being compared, any increases observed in π_m could not be positively attributed to the effects of exit area constriction.

Because the maximum total mass flow through the ejector occurs when the mixed flow at the exit reaches sonic velocity, the maximum constriction ratio is chosen such that when operating at this critical condition $\alpha = 0.75$. For all lesser degrees of constriction, the exit pressure is set to a value producing the same value for α as the maximum constriction case but which is generally above that required to choke the mixed exit flow. For the completely unconstricted case, this results in the flowfield shown in Fig. 7a.

The remaining major ejector parameters are independent of the ejector duct configuration, as σ depends only on the inflow geometry and both θ and ζ depend on the *total* conditions entering the ejector, which remain constant between all cases considered (see Tables 1 and 2).

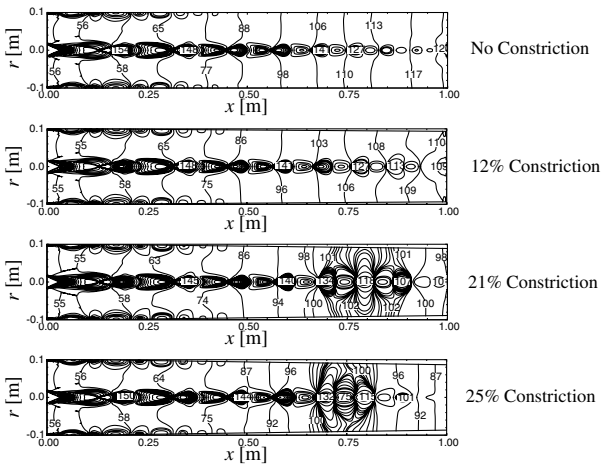

Fig. 9 Static pressure contours (kPa) within the ejector for various degrees of exit area constriction.

Table 3 Ejector exit properties for various degrees of constriction

Variable	1-D theory, 0%	0%	12%	21%	25%
α	0.75	0.75	0.76	0.76	0.75
M_m	0.46	0.53	0.66	0.80	0.96
π_m	2.83	2.24	2.33	2.50	2.75
$\bar{\pi}_m$	——	1.00	1.04	1.11	1.23

Figure 8a shows the first constriction strategy considered, a conically constricting duct where the outer wall angle is set such that the desired area is obtained at the exit plane of a 1.0 m long ejector. For the three constriction ratios considered (12, 21, and 25%), Fig. 8b shows the increase in the mixed flow Mach number required to maintain $\alpha = 0.75$ as the exit area is decreased. As shown, the mixed flow Mach number for the case with the highest degree of constriction is approximately constant at a value of unity, which indicates that this configuration is operating under maximum mass flow conditions. Therefore, cases in which the exit area is constricted by more than 25% are not considered because it is impossible to set the ratio of air to rocket exhaust mass flows at 3:4 for the operating conditions listed in Table 2. Also shown is the Mach number profile of the unconstricted base configuration, where on a mass-flow-averaged basis, a value of 0.53 indicates the existence of a substantial degree of subsonic flow within the ejector (also seen in Fig. 7a).

The flowfields within the four ejector configurations considered are shown in Fig. 9. The uniformity of the entrained air static pressure at approximately 55 kPa indicates the success to which setting the exit plane pressure is used to control the entrained air inflow conditions (because only the stagnation conditions are held constant on the inflow boundary). The difference in the back pressures required to achieve this constant value of α can also be seen, where the unconstricted case has a back pressure of approximately 120 kPa compared to approximately 87 kPa for the case in which the area is constricted by 25%.

To determine the compression ratio while avoiding any artificial inflation in π_m due to the inclusion of the unmixed, high total pressure, central rocket core, the hatched areas shown in Fig. 10 are neglected (see [23] for details). The total pressure is then calculated on a mass-flow-averaged basis from the lowest unhatched radial position outwards. This results in approximately the central 15% of the ejector radius being neglected for all the cases considered (which is equivalent to neglecting approximately 5% of the total ejector exit area).

The resulting compression ratios are used to determine the compression augmentation values shown in Table 3 and Fig. 11a. As can be seen, increasing the degree of constriction increases the compression ratio exponentially, where despite smaller incremental decreases in exit area, the compression augmentation more than doubles between consecutive cases considered. Although the effect of the exit area decrease is minimal for a 12% constriction (approximately 4% increase in π_m), for the case in which the exit flow reaches sonic velocity the compression ratio increases by approximately 23%.

Figure 11b compares the resulting compression ratio profiles at the ejector exit plane for all the degrees of constriction considered. As shown, the size of the central rocket exhaust stream at the exit plane is approximately independent of the degree to which the exit area is

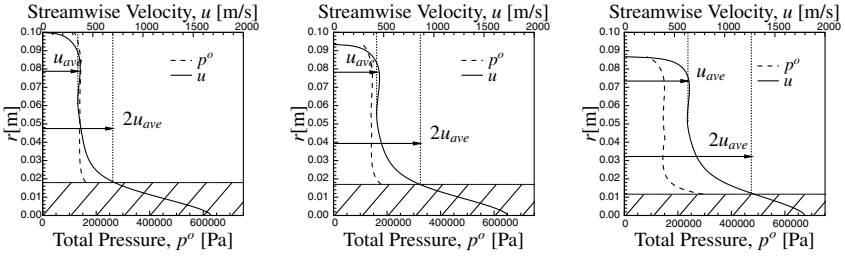

a) No constriction **b) 12% constriction** **c) 25% constriction**

Fig. 10 Determination of the lower radial bound of the mixed flow region for use in determining π_m.

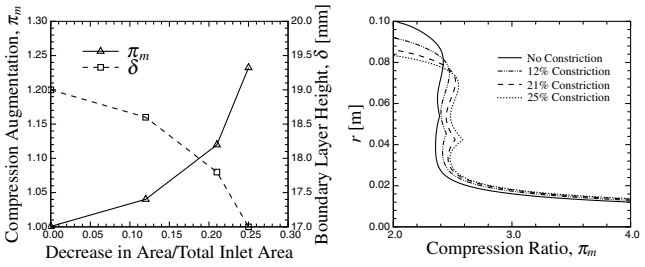

a) Massflow averaged **b) Exit profile**

Fig. 11 Comparison of compression ratio results at the exit plane of a 1.0 m ejector for various exit area constrictions.

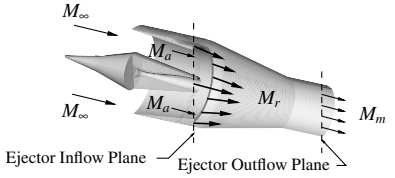

Fig. 12 Conical/cylindrical ejector configuration.

decreased. This indicates that the central rocket core contains nearly the same quantity of energy in each case and that the observed increases in the compression ratio are thus not due to a more efficient transfer of this energy to the mixed flow. However, examining the relationship between the boundary layer height and the decrease in exit area in Fig. 11a, it is observed that the greater the degree of area constriction, the smaller the resulting boundary layer at the exit plane. Thus for cases in which the angle of the outer wall promotes the annular rocket stream's penetration into the entrained air stream, more of its energy is observed to be transferred to the mixed flow region as indicated by a thinner low-energy boundary layer. It should also be noted that the decrease in boundary layer height is not an effect of decreasing the length of the surface along which the boundary layer develops, as for each degree of constriction the outer wall angle is varied (from 0.70 deg for a 12% constriction to 0.85 deg for a 25% constriction) to achieve the desired exit area over a constant length of 1 m.

Conical/Cylindrical Configuration

For all the configurations considered thus far, constriction has occurred over the length of the entire ejector as shown in Fig. 8a. However, for a given constriction ratio, the outer walls can be more severely angled to yield the required area over a length significantly shorter than the total ejector length itself. For a constant length ejector this yields the conical/cylindrical, or funnel, configuration shown in Fig. 12.

To evaluate the effects of using a constant area cylindrical section in combination with a conically converging length, the results are

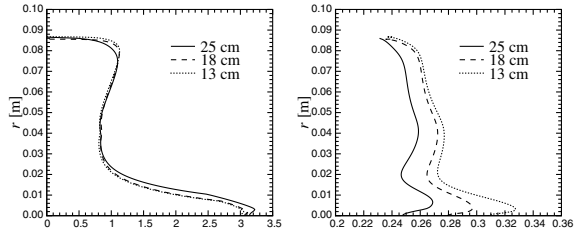

a) Mach number **b) Density [kg/m^3]**

Fig. 14 Comparison of Mach number and density profiles at the beginning of the cylindrical section.

compared with those for the configuration with a 25% area constriction. Cylindrical lengths of 13, 18, and 25 cm are placed downstream of the conical section, thereby creating ejectors that constrict over 87, 82, and 75% of their lengths, respectively, (where in all cases the exit area is decreased by 25%).

The Mach number contours for both the shortest and longest cylindrical sections are shown in Fig. 13. It should be noted that the third and fourth profiles are at different locations between Figs. 13a and 13b, where in each case the profile is located at the beginning and midpoint of the cylindrical section (which occurs at different streamwise distances depending on the length of the cylindrical section).

Examining the profiles at both the 87 and 75 cm locations in Figs. 13a and 13b, respectively, it is observed that the mixed flow makes the transition to completely sonic velocity at approximately the beginning of the cylindrical section in each case, independent of its streamwise location. Figure 14a shows this effect in more detail; the Mach number profiles at the beginning of the cylindrical sections are shown for all lengths considered. As shown, the flow is approximately choked across the entire radius, with only a small region of high subsonic flow existing between radii of approximately 3 and 6 cm. Also interesting to note, the profiles at these locations appear independent of the length of the cylindrical section used, despite the fact that the entrance to the longest section is located twice the distance from the ejector exit plane as compared to the entrance of the shortest section.

The most significant impact of this result is shown in the Mach number contours at the ejector entrance (Fig. 13), where the 13 cm configuration produces an air inflow Mach number of 0.31, approximately 24% higher than the value of 0.25 shown for the 25 cm configuration. As shown in Table 4, this results in a variation of α by as much as 15% from the case in which the constriction takes place over the entire length of the ejector. This is a direct result of the exit plane being isolated from the upstream portions of the flow by the critical condition at the entrance to the cylindrical section. Because the flow at this point has already reached sonic velocity, any downstream boundary conditions imposed at the exit serve only to alter the flow within the cylindrical section itself. The conditions at the air inflow plane are determined by the throat location as seen by

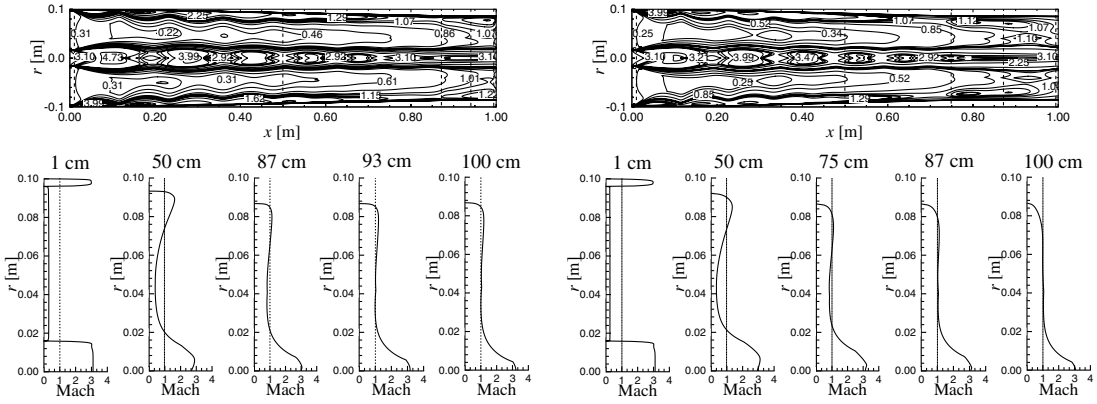

a) 13cm cylindrical section **b) 25cm cylindrical section**

Fig. 13 Mach number contours for a 13 and a 25 cm cylindrical end section.

Table 4 Ejector exit properties for configurations yielding a 25% constriction in area using various cylindrical lengths

Variable	0 cm	13 cm	18 cm	25 cm
α	0.75	0.86	0.82	0.72
M_m	0.96	1.14	1.13	0.96
π_m	2.75	2.92	2.90	2.85
$\bar{\pi}_m$	1.23	1.30	1.29	1.27

the subsonic flow, which in all cases occurs at the end of the conical section.

This is due to the fact that as the flow passes into the cylindrical section, the forced compression from the outer wall is relieved by the constant area duct. This allows the flow to turn away from the axis without further hindrance, in contrast to the continually decreasing area as observed when constriction occurs along the entire ejector length. Therefore, unlike the purely conical ejectors where the aerodynamic throat and the exit plane coincide due to the constantly decreasing area, the addition of a cylindrical section separates these two locations. With the conditions at the throat location being the dominant factor in determining the air mass flow entrained into the ejector, this separation creates a condition whereby one can no longer control α through a manipulation of the pressure at the exit plane.

The variation in α shown in Table 4 is thus due to the differences in the flow properties at the start of the cylindrical sections. Although Fig. 14a shows the Mach number profiles at the start of the cylindrical sections to be independent of the length considered, in this case this does not accurately reflect the mixing progress of the flow. As shown by the density profiles in Fig. 14b, the shorter the cylindrical section, the higher the density at the end of the conical section. This is a result of the longer length in which both the rocket and airstreams have to mix before choking when using a shorter cylindrical section. This greater mixing results in a higher density at the choke point within the ejector, which when combined with the fact that the Mach number and temperature at this location are approximately constant for all lengths considered (there is a less than 5% variation in both the temperature and mass-flow-averaged Mach number in going from a 13 to a 25 cm section), yields a higher mass flow passing through the ejector. Recalling that the rocket exhaust conditions are fixed, this requires a greater entrained air mass flow rate for the 13 cm configuration. In fact, because each cylindrical length produces a different density profile at the choke point, the value of α varies between all the cases considered. However, because an increase in the air/rocket mass flow ratio tends to *decrease* the compression ratio, the variations observed for both the 13 and 18 cm sections add a conservative effect when evaluating the compression ratio of these configurations (whereas the 25 cm configuration produces a value for α less than 3% below that observed for the purely conical ejector).

Figure 15 compares the compression augmentation results for both the conical and conical/cylindrical ejector configurations. One of the most interesting results is that it is the shortest cylindrical length that produces the highest compression augmentation, 30% higher than a similar ejector without any area constriction and still 7% higher than a conical ejector configuration with the same degree of constriction. This is despite the fact that the air/rocket mass flow ratio is nearly 15% higher when using the 13 cm cylindrical length as compared to the conical case, a factor that acts to decrease the resulting compression ratio. The augmentation values for the 18 and 25 cm configurations are also nearly 30% (29 and 27%, respectively), indicating that although the longer lengths produce a larger boundary layer, thereby decreasing π_m, this effect is approximately offset by the increase in π_m due to the decrease in α. Therefore, for the cylindrical length at which the air/rocket mass flow ratio more closely matches the value obtained using a purely conical configuration, one can expect an additional 5–7% increase in the compression ratio.

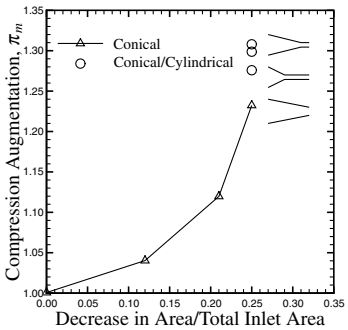

Fig. 15 Summary of compression augmentation due to area constriction.

Summary

The incorporation of an ejector section within a rocket-based propulsive device has been shown to have positive benefits on the thrust obtainable when compared to a typical pure rocket launch system. Although both the quantity of atmospheric air entrained into the ejector and the total pressure of the mixed flow at the ejector exit are shown to impact the thrust potential of an ejector-rocket system, an increase in the latter is shown to have a greater impact on performance. Theoretically it is shown that even if the entrained air mass flow is decreased by up to 60% to achieve an increase of 30% in the compression ratio, one would still obtain a 10% increase in thrust as compared to a pure rocket system.

To test the effectiveness of decreasing the ejector area as a means of increasing the compression ratio, numerical simulations are performed on both a conical and a conical/cylindrical ejector configuration. In all cases the ejector length is kept constant at five times the inlet diameter and the maximum degree of constriction is set so as to obtain a minimum value for the air/rocket mass flow ratio of 0.75. Results indicate that it is possible to achieve an increase in the compression ratio of up to 30% through a 25% decrease in the ejector area using a conical/cylindrical configuration (whereas the entrained air mass flow is decreased by less than 30% as compared to an unconstricted configuration). Further, the results show that not only the degree to which the exit area is constricted, but also the manner in which this constriction is performed, can have a significant impact on the overall compression ratio of the ejector.

Therefore, both the theoretical advantage of increased compression on ejector performance, as well as the viability of achieving this increase through the use of area constriction, are demonstrated.

Acknowledgment

This work was sponsored by the Natural Science and Engineering Research Council of Canada, whose support is greatly appreciated.

References

[1] von Kármán, T., "Theoretical Remarks on Thrust Augmentation," *Reissner Anniversary Volume: Contributions to Applied Mechanics*, edited by J. W. Edwards, P. I. of Brooklyn, Ann Arbor, MI, 1949, pp. 461–468.

[2] Fabri, J., and Siestrunck, R., "Supersonic Air Ejectors," *Advances in Applied Mechanics*, Academic Press, New York, 1958, pp. 1–34.

[3] Dutton, J., and Carroll, B., "Optimal Supersonic Ejector Designs," *Journal of Fluids Engineering*, Vol. 108, Dec. 1986, pp. 414–420.

[4] Dutton, J., and Carroll, B., "Limitation of Ejector Performance Due to Exit Choking," *Journal of Fluids Engineering*, Vol. 110, March 1988, pp. 91–93.

[5] Emanuel, G., "Optimum Performance for a Single-Stage Gaseous Ejector," *AIAA Journal*, Vol. 14, No. 9, Sept. 1976, pp. 1292–1296.

[6] Chow, W. L., and Addy, A. L., "Interaction Between Primary and Secondary Streams of Supersonic Ejector Systems and Their Performance Characteristics," *AIAA Journal*, Vol. 2, No. 4, April 1964, pp. 686–695.

[7] Chow, W. L., and Yeh, P. S., "Characteristics of Supersonic Ejector Systems with Nonconstant Area Shroud," *AIAA Journal*, Vol. 3, No. 3, March 1965, pp. 525–527.

[8] Peters, C. E., Phares, W. J., and Cunningham, T. H., "Theoretical and Experimental Studies of Ducted Mixing and Burning of Coaxial

Streams," *Journal of Spacecraft and Rockets*, Vol. 6, No. 12, Dec. 1969, pp. 1435–1441.
[9] Masuya, G., Chinzei, N., and Ishii, S., "A Study of Air Breathing Rockets-Subsonic Mode Combustion," *Acta Astronautica*, Vol. 8, Nos. 5–6, 1981, pp. 643–661.
[10] Escher, W. J. (ed.), *The Synerjet Engine: Airbreathing/Rocket Combined-Cycle Propulsion for Tomorrow's Space Transports*, PT-54, Society of Automotive Engineers, Warrendale, PA, 1997.
[11] Escher, W., and Schnurstein, R., "A Retrospective on Early Cryogenic Primary Rocket Subsystem Designs as Integrated into Rocket-Based Combined-Cycle (RBCC) Engines," AIAA Paper 93-1944, 1993.
[12] Nix, M. B., and Escher, W. J. D., "Spaceliner Class Operability Gains via Combined Airbreathing/Rocket Propulsion: Summarizing an Operational Assessment of Highly Reusable Space Transports," AIAA Paper 99-2355, 1999.
[13] Daines, R., and Segal, C., "Combined Rocket and Airbreathing Propulsion Systems for Space Launch Applications," *Journal of Propulsion and Power*, Vol. 14, No. 5, Sept.–Oct. 1998, pp. 605–612.
[14] Billig, F. S., "The Integration of the Rocket with the Ram-Scramjet as a Viable Transatmospheric Accelerator," ISABE Paper 93-7017, 1993.
[15] Fink, L. E., "High Mach Number Applications: Combined Cycles," *Tactical Missile Propulsion*, Vol. 170, Progress in Astronautics and Aeronautics, AIAA, Washington, DC, 1994, pp. 497–515.
[16] Ramette, P., Scherrer, D., and Doublier, M., "Etude Comparative de Differents Systemes de Propulsion Combinee," *AGARD Conference Proceeding 479*, AGARD, 1990, pp. 5-1–5-11.
[17] Dorrington, G. E., "Performance of Air-Breathing Single-Stage-To-Orbit Vehicles," IAF Paper 89-309, 1989.
[18] Matesanz, A., Velazquez, A., Tizon, J., and Montanes, J., "Numerical Reconstruction of Ejector Rocket Experimental Tests," *Journal of Propulsion and Power*, Vol. 18, No. 6, Nov.–Dec. 2002, pp. 1191–1198.
[19] West, J., Ruf, J., Cramer, J., Pal, S., and Santoro, R., "Computational Insight to Experimentally Observed Change in Mixing Characteristics of an RBCC Engine in Ejector Mode," AIAA Paper 2001-3459, 2001.
[20] Ruf, J. H., "Benchmark of FDNS CFD Code for Direct Connect RBCC Test Data," AIAA Paper 2000-36875, 2000.
[21] Jahingir, M. N., and Huque, Z., "Design Optimization of Rocket-Based Combined-Cycle Inlet/Ejector System," *Journal of Propulsion and Power*, Vol. 21, No. 4, July–Aug. 2005, pp. 650–655.
[22] Cramer, J. M., Greene, M., Pal, S., and Santoro, R. J., "RBCC Ejector Mode Operating Characteristics for Single and Twin Thruster Configurations," AIAA Paper 2001-3464, 2001.
[23] Etele, J., Sislian, J. P., and Parent, B., "Effect of Rocket Exhaust Configurations on Ejector Performance in RBCC Engines," *Journal of Propulsion and Power*, Vol. 21, No. 4, July–Aug. 2005, pp. 656–666.
[24] Makaron, V., and Fedyayev, Y. G., "Organization of Working Process in Liquefied Air Cycle Rocket-Ramjet Engine," AIAA Paper 96-4522, 1996.
[25] Daines, R. L., "Numerical Analysis of High-Frequency Jet-Switching on Dynamic Ejector Flowfields," AIAA Paper 97-2757, 1997.
[26] Daines, R. L., and Bulman, M., "Computational Analyses of Dynamic Rocket Ejector Flowfields," AIAA Paper 96-2686, 1996.
[27] Aoki, S., Lee, J., Masuya, G., Kanda, T., and Kudo, K., "Aerodynamic Experiment on an Ejector-Jet," *Journal of Propulsion and Power*, Vol. 21, No. 3, May–June 2005, pp. 496–503.
[28] Kanda, T., and Kudo, K., "Conceptual Study of a Combined-Cycle Engine for an Aerospace Plane," *Journal of Propulsion and Power*, Vol. 19, No. 5, 2003, pp. 859–867.
[29] Etele, J., "Computational Study of Variable Area Ejector Rocket Flowfields," Ph.D. Thesis, Univ. of Toronto, Institute for Aerospace Studies, Toronto, 2004.
[30] Parent, B., and Sislian, J. P., "The Use of Domain Decomposition in Accelerating the Convergence of Quasi-Hyperbolic Systems," *Journal of Computational Physics*, Vol. 179, No. 1, 2002, pp. 140–169.
[31] Parent, B., "Computational Study of Fuel Injection in a Shcramjet Inlet," Ph.D. Thesis, University of Toronto, Toronto, 2002.
[32] Parent, B., and Sislian, J. P., "Validation of the Wilcox $k\omega$ Model for Flows Characteristic to Hypersonic Airbreathing Propulsion," *AIAA Journal*, Vol. 42, No. 2, 2004, pp. 261–270.
[33] Wilcox, D. C., *Turbulence Modeling for CFD*, 2nd ed., DCW Industries, Inc., La Canada, CA, 1998.

J. Martin
Associate Editor